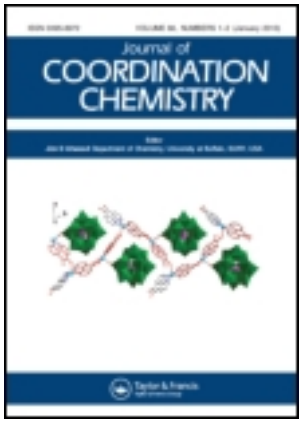

Journal of Coordination Chemistry
Publication details, including instructions for authors and subscription information:
http://www.tandfonline.com/loi/gcoo20

Spectroscopic, structure, and DFT studies of cationic palladium(II) complexes with imidazole derivative ligands

J.G. Małecki [a]

[a] Department of Crystallography , Institute of Chemistry, University of Silesia , Katowice , Poland

Accepted author version posted online: 18 Mar 2013.Published online: 19 Apr 2013.

To cite this article: J.G. Małecki (2013) Spectroscopic, structure, and DFT studies of cationic palladium(II) complexes with imidazole derivative ligands, Journal of Coordination Chemistry, 66:9, 1561-1573, DOI: 10.1080/00958972.2013.784903

To link to this article: http://dx.doi.org/10.1080/00958972.2013.784903

Journal of Coordination Chemistry, 2013
Vol. 66, No. 9, 1561–1573, http://dx.doi.org/10.1080/00958972.2013.784903

Spectroscopic, structure, and DFT studies of cationic palladium(II) complexes with imidazole derivative ligands

J.G. MAŁECKI*

Department of Crystallography, Institute of Chemistry, University of Silesia, Katowice, Poland

(*Received 18 July 2012; in final form 7 January 2013*)

Two palladium(II) complexes with imidazole derivative ligands have been synthesized. The molecular structures of the complexes were determined by X-ray crystallography and their spectroscopic properties were studied. Based on the crystal structures, computational investigations were carried out to determine the electronic structures of the complexes. The electronic spectra were calculated with use of time-dependent DFT method, and the transitions were correlated with the molecular orbitals of the complexes. The emission of the complex with 1-methylimidazole was examined.

Keywords: Palladium(II) complexes; Imidazo[12-*a*]pyridine; 1-Methylimidazole; X-Ray structure; UV–Vis; Luminescence; DFT; TD-DFT

1. Introduction

Palladium(II) complexes attract interest because of their potentially beneficial pharmacological properties. Palladium complexes with aromatic N-containing ligands, for example, derivatives of pyridine, quinoline, pyrazole, and 1,10-phenanthroline, have promising antitumor characteristics [1–4]. Some of these complexes, especially the *trans* analogs with nonplanar heterocyclic amine ligands, have overcome multi-factorial cisplatin resistance in human ovarian cell lines [5, 6]. Pd(II) complexes have also been widely explored due to their catalytic efficiency, for example, for various carbon-carbon and carbon-nitrogen bond formations [7–11]. While most studies of palladium have concentrated on the reactivity of its complexes, little information about their electronic structures has been obtained, despite four-coordinate palladium(II) complexes with square-planar geometry having a large class of useful building blocks for producing interesting molecular structures by combination of coordination chemistry and hydrogen bonding [12].

Complexes with N-heteroaromatic ligands and metals such as ruthenium(II), osmium(II), and rhenium(I) are studied due to their luminescent properties. In contrast, d^8 metal complexes have been much less studied. The luminescent properties of palladium(II) complexes strongly depend on their electronic structure. For this reason, the study of the electronic structures of such complexes is valuable as a way to predict their properties [13, 14].

*Email: gmalecki@us.edu.pl

Here, an experimental and quantum chemical study of two cationic palladium(II) complexes with imidazole ligands is reported. The quantum chemical study included characterization of the molecular and electronic structures of the complex by analysis of optimized molecular geometry, electronic populations by using the natural bond orbitals (NBOs) scheme. The latter was used to identify the nature of the interactions between the ligands and palladium. The calculated density of states (DOS) showed the interactions and influences of the orbital composition in the frontier electronic structure. The time-dependent density functional theory (TD-DFT) was finally used to calculate the electronic absorption spectrum. Based on a molecular orbital scheme, these results allowed the interpretation of the UV–Vis spectrum obtained at an experimental level.

2. Experimental

All reagents used for the synthesis of the complexes were commercial products and have been used without purification.

2.1. *Synthesis of [Pd(L)$_4$]Cl$_2$ complexes*

A typical procedure for preparation of the complexes is as follows. A solution of $PdCl_2$ (0.177 g, 0.1 mM), imidazo[1,2-α]pyridine (**1**) (0.41 cm^{-3}, 0.4 mM) and 1-methylimidazole (**2**) (0.45 cm^{-3}, 0.4 mM) in acetonitrile (50 cm^3) was refluxed for 3 h and then filtered. Crystals suitable for X-ray analysis were obtained by crystallization of the crude product of **1** from chloroform and slow evaporation of solvent from **2**.

1: IR (KBr) [cm^{-1}]: 3123 ν_{ArH}; 2907 ν_{CH}; 1621 $\nu_{C=C}$; 1568 $\nu_{C=N}$; 1452, 1306 $\delta_{(C–CH\ in\ the\ plane)}$; 1434, 1242 ν_{Ph}; 1109, 1050 δ_{CH}; 907, 837 $\delta_{(C–H\ out\ of\ the\ plane)}$; 754, 656, 612 $\delta_{(C–C\ out\ of\ the\ plane)}$. ^{1}H NMR [$\delta$, ppm]: (DMSO-d^6): 8.712 (s, H3), 8.617 (d, H2; J = 5.2 Hz), 8.264 (s, H1), 7.882 (d, H6; J = 7.9 Hz), 7.490 (dd, H5; J = 7.8, 5.7), 5.579 (s, H4). UV-vis [λ nm, (ε)] (acetonitrile): 380, 311, 280, 236, 202.

2: IR (KBr) [cm^{-1}]: 3436, 3380 ν_{water}; 3103, 3052 ν_{ImH}; 2921, 2823 ν_{CH}; 2100, 1726 (ν_{water}), 1626, 1605 $\nu_{C=C}$, $\nu_{C=N}$; 1539, 1527; 1419, 1292 $\delta_{(C–CH\ in\ the\ plane)}$; 1242, 1119, 1105 δ_{CH}; 967 $\delta_{(C–H\ out\ of\ the\ plane)}$; 837 $\delta_{(C–C\ out\ of\ the\ plane)}$; 764, 660; 622 $\delta_{(C–C\ out\ of\ the\ plane)}$; 484 $\nu_{Pd–N}$. ^{1}H NMR [δ, ppm]: (DMSO-d^6): 8.30 (s), 8.21 (s), 8.05 (d, J = 26.8 Hz), 8.01 (s), 7.56 (s), 7.41 (s), 7.32 (d, J = 15.4 Hz), 7.26 (s), 7.16 (dd, J = 27.1, 11.8 Hz), 7.03 (s), 6.87 (s), 6.74 (s, H_2O), 3.71 (s, CH_3), 3.64 (s, CH_3), 3.37 (s, CH_3), 2.51 (H_2O). UV-vis [λ nm, (ε)] (acetonitrile): 317, 275, 232, 210.

2.2. *Physical measurements and DFT calculations*

Infrared spectra were recorded on a Perkin Elmer FT-IR spectrophotometer from 4000 to 450 cm^{-1} using KBr pellets. Electronic spectra were measured on a Lab Alliance UV-vis 8500 spectrophotometer from 700 to 180 nm in methanol. ^{1}H NMR spectra were obtained at room temperature in DMSO-d^6 using a Bruker 400 spectrometer. Luminescence measurement was made in methanol on an F-2500 FL spectrophotometer at room temperature.

Calculations were carried out using the Gaussian09 [15] program. The DFT/B3LYP [16, 17] method was used for geometry optimization and electronic structure determination.

The electronic spectra were calculated by the TD-DFT [18] method. The calculations were performed using the DZVP basis set [19] with functions with exponents 1.94722036 and 0.748930908 on palladium and polarization functions for all other atoms: 6-31G** for carbon, nitrogen and 6-31G for hydrogen. The PCM solvent model was used in the Gaussian calculations with acetonitrile as the solvent. NBO calculations were performed with the NBO code [20] included in Gaussian09. GaussSum 2.2 [21] was used to calculate group contributions to the molecular orbitals and to prepare the partial DOS and overlap population density of states (OPDOS) spectra. The contribution of a group to a molecular orbital was calculated using Mulliken population analysis. The PDOS and OPDOS spectra were created by convoluting the molecular orbital information with Gaussian curves of unit height and FWHM of 0.3 eV.

2.3. *Crystal structure determination and refinement*

Crystals of $[Pd(Impy)_4]Cl_2 \cdot 2CHCl_3$ (**1**) and $[Pd(ImCH_3)_4]Cl_2 \cdot 2H_2O$ (**2**) were mounted on an Xcalibur, Atlas, Gemini ultra Oxford Diffraction automatic diffractometer equipped with a CCD detector and used for data collection. X-ray intensity data were collected with graphite monochromated MoK_α radiation ($\lambda = 0.71073$ Å) at 295.0(2) K, with ω scan mode. Ewald sphere reflections were collected up to $2\theta = 50.10°$. The unit cell parameters were determined from least-squares refinement of the setting angles of 4539 and 4920 strongest reflections. Details concerning crystal data and refinement are gathered in table 1. Lorentz, polarization and empirical absorption correction using spherical harmonics implemented in SCALE3 ABSPACK scaling algorithm [22] were applied. The structure was solved by the Patterson method and subsequently completed by difference Fourier recycling. All nonhydrogen atoms were refined anisotropically using full-matrix, least-squares. All hydrogens were found from difference Fourier synthesis after four cycles of anisotropic refinement and refined as "riding" on the adjacent carbon with individual isotropic temperature factor 1.2 times the value of the equivalent temperature factor of the parent atom. The Olex2 [23] and SHELS97, SHELXS97 [24] programs were used for all the calculations.

3. Results and discussion

The cationic palladium(II) complexes with imidazole derivative ligands were obtained by reactions of $PdCl_2$ with imidazo[1,2-α]pyridine (**1**) and 1-methylimidazole (**2**) in acetonitrile. The crude product of **1** obtained from the reaction was recrystallized from chloroform to get crystals suitable for X-ray analysis. In IR spectra of the complexes, the ring C=N stretch of the ligands are present at 1621–1568 cm^{-1}. The infrared spectra of imidazo [1,2-α]pyridine and 1-methylimidazole have C=N stretches at 1529 and 1534 cm^{-1}, respectively. The coordination of the ligands to palladium results in shift of these bands to higher frequencies. The IR spectrum of **2** has bands connected with waters of crystallization (3436–3380 cm^{-1} and 2100, 1726 cm^{-1}) (Supplementary material). ^1H NMR spectra of the complexes display the sets of signals from the ligands given in experimental section of the article. The spectra are complicated and were calculated using DFT method. Figure 1 presents the aromatic part of the experimental ^1H NMR spectrum of **2**. The NMR calculations were carried out at density functional B3LYP level using 6-311G(d) basis set based on energy-minimized structures of the complex generated in the geometry optimization step of the calculation. The gage-independent atomic orbital method was adopted in the

Table 1. Crystal data and structure refinement details of **1** and **2**.

	1	**2**
Empirical formula	$C_{28}H_{24}N_8Pd$, 2($CHCl_3$), 2(Cl)	$C_{16}H_{24}N_8Pd$, 2(H_2O), 2(Cl)
Formula weight	888.59	541.76
Temperature [*K*]	295(2) K	295.0(2) K
Crystal system	Orthorhombic	Monoclinic
Space group	*P*bca	$P2_1/n$
Unit cell dimensions		
a [Å]	16.0834(5)	9.2791(5)
b [Å]	11.6681(4)	18.1234(11)
c [Å]	19.3203(7)	13.9924(8)
α	90	90
β	90	98.489(5)
γ	90	90
Volume [Å^3]	3625.7(2)	2327.3(2)
Z	4	4
Calculated density [Mg m^{-3}]	1.628	1.546
Absorption coefficient [mm^{-1}]	1.137	1.055
F(000)	1776	1104
Crystal dimensions [mm]	0.40 × 0.13 × 0.10	0.27 × 0.18 × 0.10
θ range for data collection [°]	3.49 to 25.05	3.60 to 25.05
Index ranges	−14 <= h <= 19	−11 <= h <= 11
	−10 <= k <= 13	−21 <= k <= 21
	−14 <= l <= 23	−16 <= l <= 16
Reflections collected	9035	13,301
Independent reflections	3187 [$R_{(int)}$ = 0.0244]	4107 [$R_{(int)}$ = 0.0281]
Data/restraints/parameters	3187/0/214	4107/0/282
Goodness-of-fit on F^2	0.994	1.042
Final *R* indices [$I > 2\sigma(I)$]	R_1 = 0.0291	R_1 = 0.0289
	wR_2 = 0.0723	wR_2 = 0.0707
R indices (all data)	R_1 = 0.0503	R_1 = 0.0289
	wR_2 = 0.0753	wR_2 = 0.0764
Largest diff. peak and hole	0.682 and −0.671	0.311 and −0.580

process [25]. The geometry of tetramethylsilane (TMS) was also optimized at the B3LYP/6-311 g(d) level and its NMR shielding tensor was calculated at the B3LYP level using the same basis set. Chemical shifts of the target complexes relative to TMS were obtained from the differences between shielding tensors of the corresponding complexes and TMS [26].

The complexes crystallize in the orthorhombic *P*bca and monoclinic $P2_1/n$ space groups, respectively. Their molecular structures are shown in figure 2. Selected bond lengths and angles are listed in table 2. Palladium(II) is square planar with the ligands bonded to the metal center through the imidazole nitrogens. In the structure of **1,** palladium is located on an inversion center, and thus, the asymmetric unit contains one half of the complex. The Pd–N distances are similar and comparable with other palladium(II) complexes. The complex molecules are stabilized by inter- and intramolecular hydrogen bonds as collected in table 3. Additionally, in **2,** the short interactions between hydrogens of methyl and imidazole rings ($1/2+x$; $1/2-y$; $-1/2+z$) with average distance 2.838 Å stabilize the crystal structure (figure 3(a)). The graph-set analysis [27] made with Mercury 3.0 [28] gave no hydrogen bond motif in the structure of **1**; in the crystal structure of **2** the hydrogen bond subset composed from bonds between water and chloride occurred as can be seen in figure 3(b). The motifs presented in figure 3(b) are composed of four dimers of $D_1^1(2)$ type, two $D_2^1(3)$ and two $D_2^2(5)$ between chloride and water.

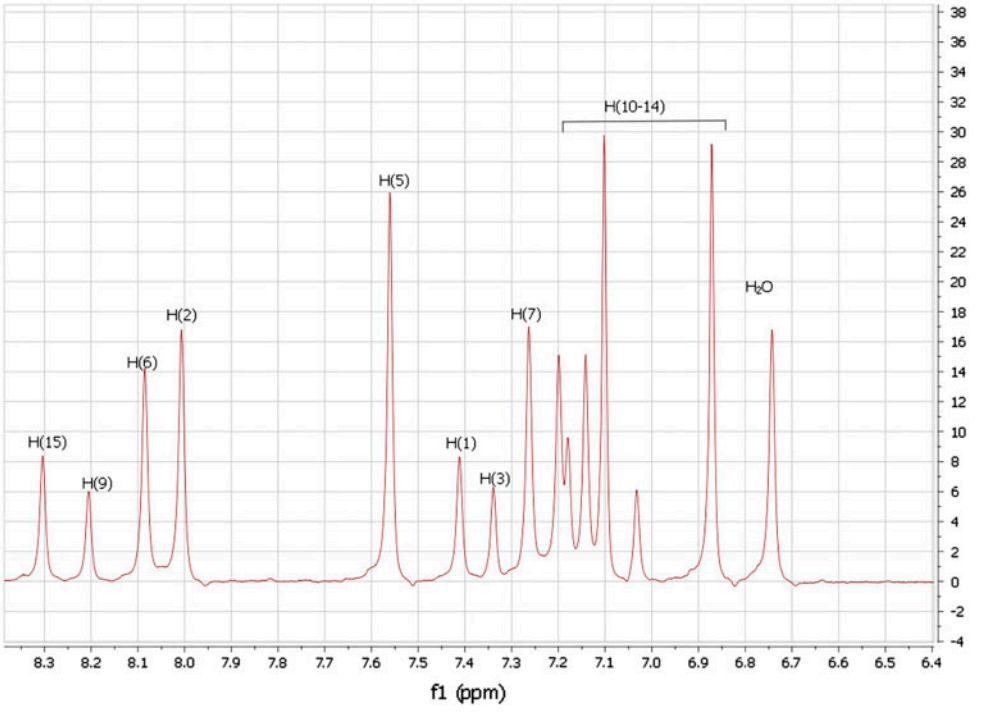

Figure 1. Aromatic part of ^{1}H NMR spectrum of **2**.

3.1. *Electronic structure*

To gain insight into the electronic structures and bonding properties of these complexes, DFT calculations were carried out. Prior to the calculations of electronic structures of the complexes, their geometries were optimized in singlet states using the B3LYP functional. For each complex, a frequency calculation was carried out, verifying that the obtained optimized molecular structure corresponds to an energy minimum, and thus, only positive frequencies were expected. The experimental IR spectrum and calculated IR transitions (Supplementary Material) show good agreement and the differences mainly result from neglecting intermolecular interactions. The differences between observed (experimental) and calculated C=N and C=C stretches are only 5 cm^{-1}. The calculations were carried out for gas phase molecules (without solvent) and in general, the predicted bond lengths and angles are elongated by about 0.1 Å and 2°, respectively. Nevertheless the general trends observed in the experimental data are reproduced by the calculations (table 2). Bond lengths are almost unchanged in the calculated gas phase structures, while the change in bond angles does not exceed 2°. Based on the optimized geometries of the complexes, NBO analyses were performed which revealed the nature of coordination between palladium and the ligands directly interacting with it. This methodology also gave a better understanding of the optimized molecular structures. From the analyses, it was found that imidazo[1,2-α]pyridine and 1-methylimidazole ligands show covalent bonding with palladium which is visible in the calculated Wiberg indices, whose values are 0.40 and 0.47 for **1** and **2**, respectively. Moreover, 1-methylimidazole presents more covalent interaction with palladium than imidazo[1,2-α]pyridine.

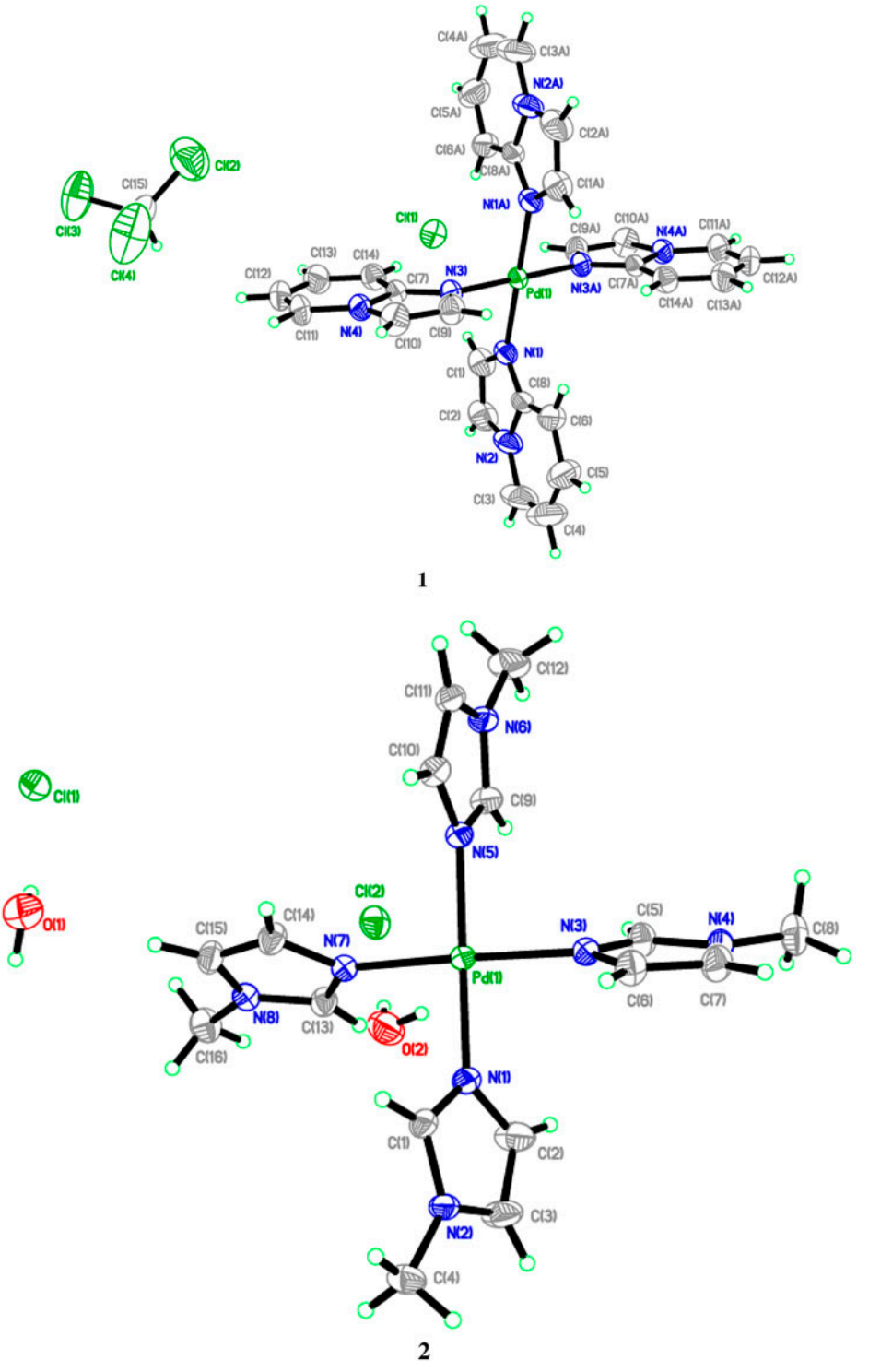

Figure 2. ORTEP drawing of **1** and **2** with 30% probability displacement ellipsoids.

Table 2. Selected bond lengths [Å] and angles [°] for **1** and **2** with the optimized geometry values.

	1		**2**	
	exp	calc	exp	calc
Bond lengths [Å]				
Pd(1)–N(1)	2.005(2)	2.058	1.998(2)	1.862
Pd(1)_N(3)	2.012(2)	2.060	2.011(2)	1.862
Pd(1)_N(5)			2.015(2)	1.862
Pd(1)_N(7)			2.008(2)	1.862
Angles [°]				
N(1)_Pd(1)_N(3)	89.64(9)	90.26	88.53(9)	89.75
N(1)_Pd(1)_N(5)			177.45(9)	179.08
N(1)_Pd(1)_N(7)			90.00(9)	89.32
N(3)_Pd(1)_N(5)			90.55(9)	90.37
N(7)_Pd(1)_N(5)			91.07(9)	90.55

Table 3. Hydrogen bonds for **1** and **2** (Å and °).

D–H···A	d(D–H)	d(H···A)	d(D···A)	∠(DHA)
1				
C(3)–H(3)...Cl(1)#1	0.93	2.74	3.609(4)	156.2
C(6)–H(6)...Cl(1)#2	0.93	2.68	3.584(3)	163.6
C(14)–H(14)...Cl(1)	0.93	2.70	3.609(3)	165.0
C(15)–H(15)...Cl(1)#3	0.98	2.41	3.372(3)	167.2
2				
O(1)–H(1A)...Cl(1)	0.70(5)	2.56(5)	3.223(4)	158(5)
O(1)–H(1B)...Cl(2)#4	0.83(5)	2.43(5)	3.247(4)	170(5)
O(2)–H(2A)...Cl(2)	0.72(6)	2.53(6)	3.246(5)	174(6)
O(2)–H(2B)...Cl(1)#5	0.86(5)	2.35(5)	3.200(5)	171(5)
C(1)–H(1)...O(1)#6	0.93	2.34	3.250(4)	165.9
C(4)–H(4C)...Cl(2)#5	0.96	2.71	3.570(3)	149.4
C(15)–H(15)...O(1)	0.93	2.59	3.412(5)	147.1

Symmetry transformations used to generate equivalent atoms: #1 $1/2+x$, $3/2-y$, $1-z$; #2 $1-x$, $2-y$, $1-z$; #3 $1-x$, $1-y$, $1-z$; #4 $3/2-x$, $-1/2+y$, $1/2-z$; #5 $1/2+x$, $1/2-y$, $1/2+z$; #6 $1-x$, $-y$, $1-z$.

The charge donations from the ligands to palladium(II) in the complexes were obtained from NBO analysis (*Second-Order Perturbation Theory Analysis*). The energy values of charge transfer were estimated at 137.52 and 198.59 kcal M^{-1} for the ligand to metal donations and 15.72 and 33.17 kcal M^{-1} for Pd→Im reverse processes for **1** and **2**, respectively. Donations from imidazole ligands to Pd(II) exceeded back donations from metal to ligand and the charges on the palladium are lower than the formal + 2 charge (0.78 for **1** and 0.64 for **2**). The natural populations of palladium 4d valence orbitals are as follows: d_{xy}1.85, d_{xy}1.90, d_{yz}1.87, $d_{x^2-y^2}$1.74, $d_z^2$1.44 in **1** and d_{xy}1.06, d_{xz}1.96, d_{yz}1.96, $d_{x^2-y^2}$1.87, $d_z^2$1.90 in **2** and total palladium valence populations are 9.25 and 9.33. Additionally, these data suggest that $ImCH_3$ is a stronger σ-donor and π-acceptor than the Impy. To compare the strength of the imidazo[1,2-α]pyridine and 1-methylimidazole ligands, DOS calculations were performed. The OPDOS diagrams gives an indication of the bonding, nonbonding and antibonding characteristics with respect to particular fragments. Analysis of the OPDOS diagram allows us to determine the donor–acceptor properties of the ligands. Figure 4 presents the interactions between palladium and imidazole type ligands (OPDOS diagrams) from which it can be seen that 1-methylimidazole is a stronger ligand than

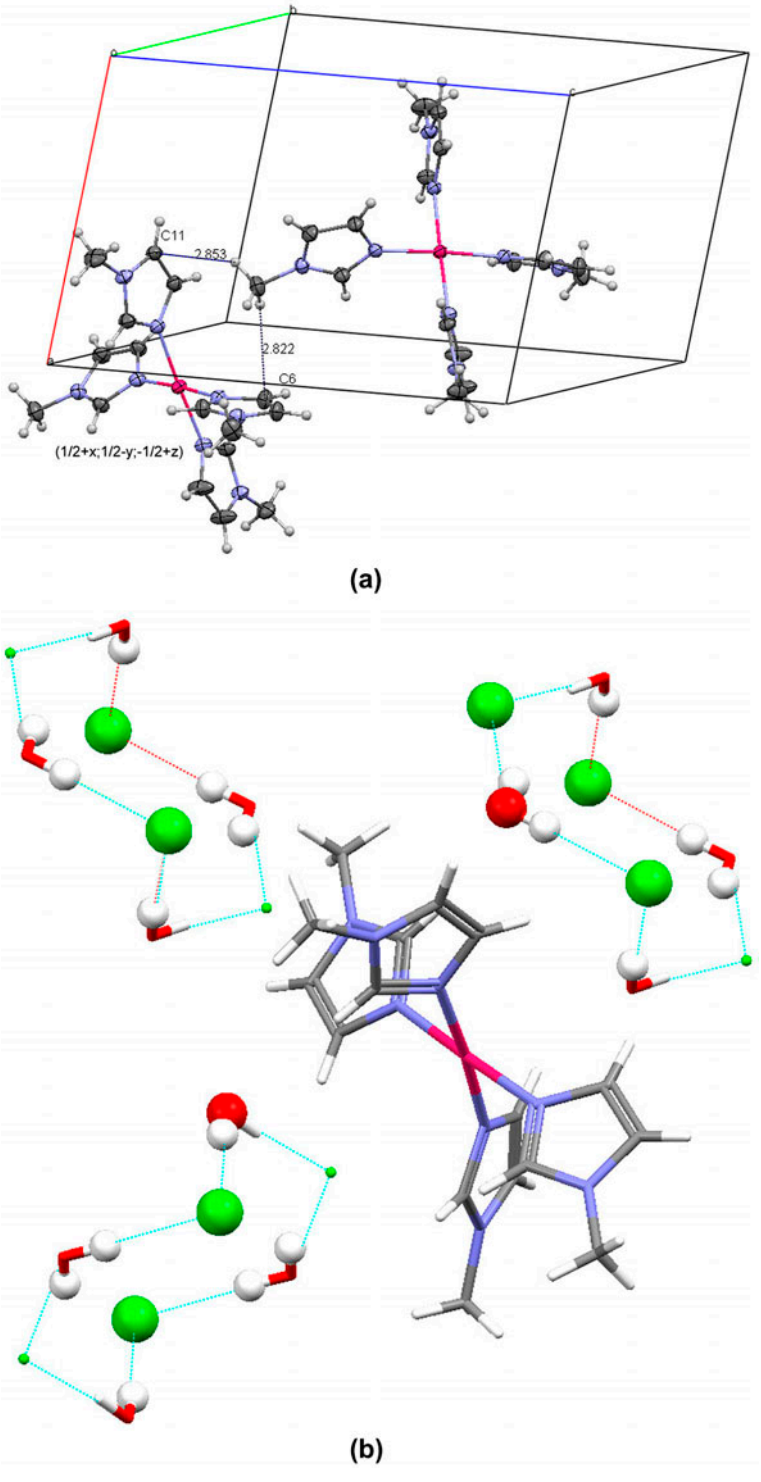

Figure 3. Intermolecular interactions in the structure of **2**: (a) short contacts between CH_3 and imidazole rings; (b) the H_2O-Cl graph-set assignment.

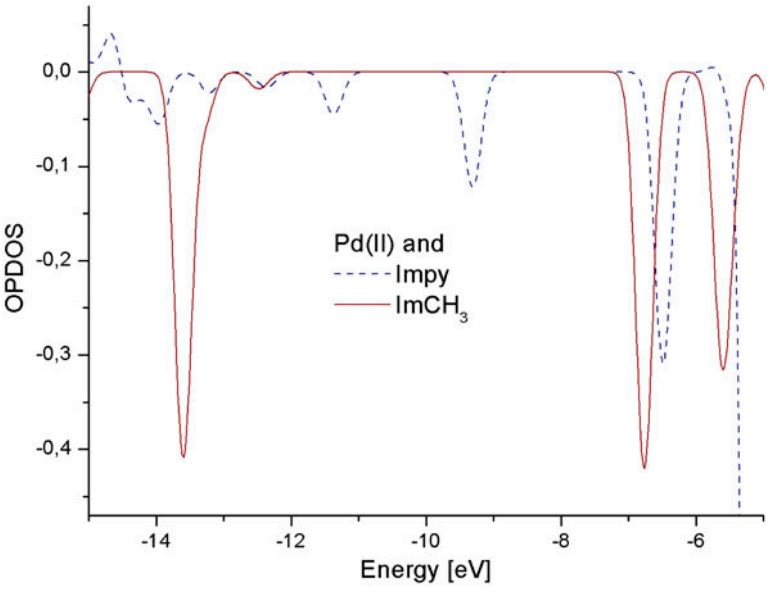

Figure 4. Overlap partial DOS diagrams of interaction of Impy and $ImCH_3$ ligands with palladium(II).

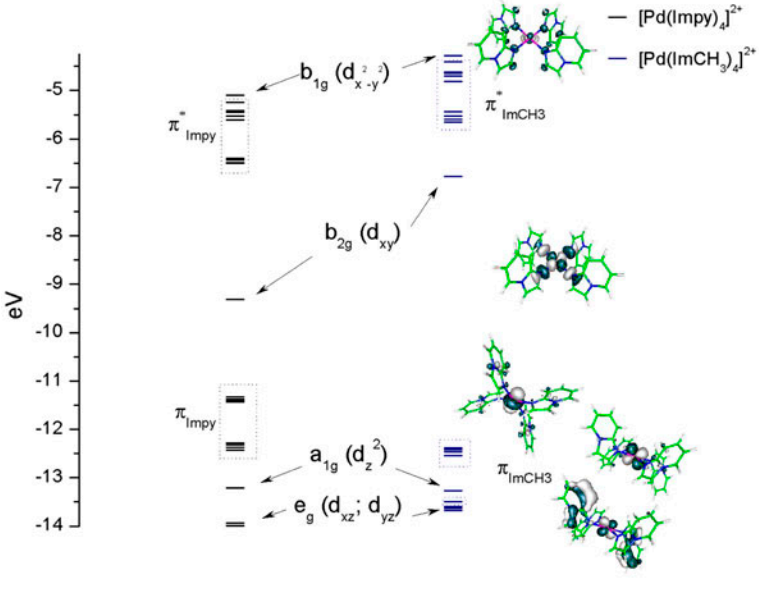

Figure 5. Simplified molecular orbital diagrams for **1** and **2**.

imidazo[1,2-α]pyridine, consistent with the charges on palladium given above. It is connected with an increase in energy of the HOMO associated with strong donor properties and strong π-acceptor ability of the ligand. Simplified molecular diagrams of the complexes are presented in figure 5. The splitting of d palladium orbitals is specific to

square planar D_{4h} symmetry of the complexes. The e_g, a_{1g}, b_{2g} and b_{1g} terms consist mainly of the palladium d orbitals with some admixture of N-heteroaromatic ligand orbitals.

3.2. *Electronic spectra*

In UV-vis spectra of the complexes, bands with maxima at 380, 311, 280, 236, 202, and 317, 275, 232, 210 nm are visible. The nature of the electronic transitions has been analyzed using TDDFT based on the optimized singlet state geometry. Electronic transitions were calculated using the long range corrected version of the B3LYP functional – CAM-B3LYP which employs the Coulomb-attenuating method. This functional provides a better estimation of excitation energies and oscillator strengths, especially for transitions with charge-transfer character. In table 4, several calculated electronic transitions and their assignments to experimental absorption bands are summarized. The assignment of the calculated orbital excitations to experimental bands was based on an overview of the composition and relative energy to the HOMO and LUMO orbitals involved in the electronic transitions.

Ligand-to-Metal Charge Transfer transitions are dominant in electronic spectra of the complexes. However, in **1** charge transfer transitions from imidazo[1,2-α]pyridine to b_{1g} term ($\pi_{impy} \rightarrow d_{x^2-y^2}/\pi^*_{impy}$) play a significant role in the energy range up to 290 nm. The transitions between e_g/a_{1g} and b_{1g} terms are calculated at high energy (222.3 nm), and in

Table 4. Calculated electronic transitions and their assignments to the experimental absorption bands for **1** and **2**.

The most important orbital excitations	Character	λ[nm]	f	Exp. λ[nm]
1				
H–3→LUMO (98%)	$\pi_{impy} \rightarrow d_{x^2-y2}/\pi^*_{impy}$	422.4	0.0031	380
H–11→LUMO (19%); H–1→LUMO (49%)	$\pi_{impy} \rightarrow d_{x^2-y2}/\pi^*_{impy}$	359.3	0.0	
H–4→LUMO (98%)	$\pi_{impy} \rightarrow d_{x^2-y2}/\pi^*_{impy}$	307.5	0.0038	311
H–6→LUMO (86%)	$\pi_{impy} \rightarrow d_{x^2-y2}/\pi^*_{impy}$	293.9	0.0	
H–3→L+4 (17%); H–2→L+1 (20%); H–1→L+3 (19%); HOMO→L+2 (24%)	$\pi_{impy} \rightarrow \pi^*_{impy}$	258.7	0.9045	280
H–3→L+1 (20%); H–2→L+4 (18%); H–1→L+2 (22%); HOMO→L+3 (21%)	$\pi_{impy} \rightarrow \pi^*_{impy}$	258.5	0.7314	
H–3→L+8 (11%); H–2→L+6 (13%); H–1→L+7 (12%); HOMO→L+5 (14%)	$\pi_{impy} \rightarrow \pi^*_{impy}$	237.4	0.1379	236
H–15→LUMO (17%); H–12→LUMO (53%)	$e_g/a_{1g}/\pi_{impy} \rightarrow d_{x^2-y^2}/\pi^*_{impy}(b_{1g})$	222.3	0.5074	
H–3→L+1 (15%); H–2→L+4 (12%); H–1→L+2 (38%)	$\pi_{impy} \rightarrow \pi^*_{impy}$	209.4	0.0034	202
2				
H–4→LUMO (83%)	$b_{2g}/\pi_{ImCH} \rightarrow d_{x^2-y^2}/\pi^*_{ImCH}(b_{1g})$	334.2	0.0004	
H–13→LUMO (15%); H–5→LUMO (58%); H–1→LUMO (12%)	$a_{1g}/\pi_{ImCH} \rightarrow d_{x^2-y^2}/\pi^*_{ImCH}(b_{1g})$	306.2	0.0004	310
H–10→LUMO (33%); H–6→LUMO (53%)	$a_{2g}/\pi_{ImCH} \rightarrow d_{x^2-y^2}/\pi^*_{ImCH}(b_{1g})$	279.0	0.0024	275
H–2→LUMO (27%); HOMO→LUMO (67%)	$\pi_{ImCH} \rightarrow d_{x^2-y^2}/\pi^*_{ImCH}(b_{1g})$	211.2	0.0015	
H–2→LUMO (67%); HOMO→LUMO (24%)	$\pi_{ImCH} \rightarrow d_{x^2-y^2}/\pi^*_{ImCH}(b_{1g})$	210.2	0.0086	210
H–3→LUMO (32%); H–1→LUMO (58%)	$\pi_{ImCH} \rightarrow d_{x^2-y^2}/\pi^*_{ImCH}(b_{1g})$	207.1	0.0001	
H–5→LUMO (18%); H–3→LUMO (53%); H–1→LUMO (17%)	$\pi_{ImCH} \rightarrow d_{x^2-y^2}/\pi^*_{ImCH}(b_{1g})$	203.2	0.002	

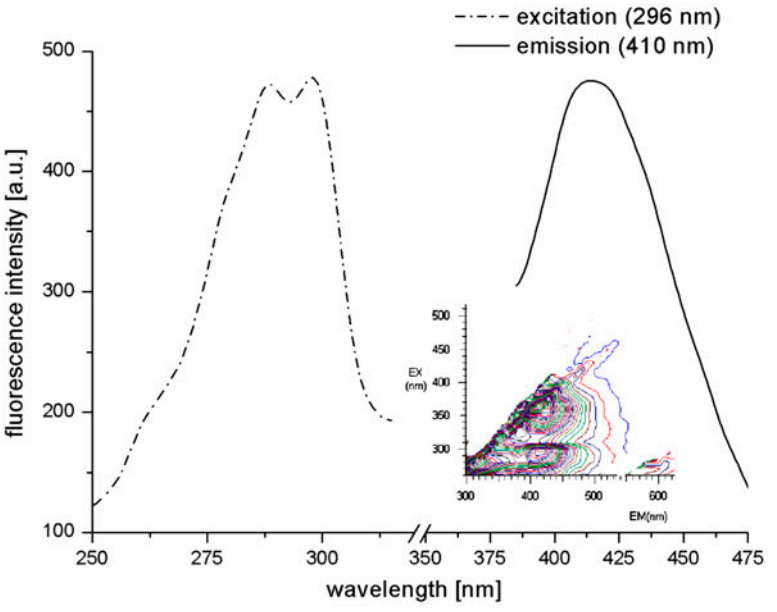

Figure 6. Fluorescence spectrum of acetonitrile solution of **2**.

this energy region, *Ligand-to-Ligand Charge Transfer* processes ($\pi_{\text{impy}} \rightarrow \pi^*_{\text{impy}}$) are predominant. In the case of electronic spectrum of **2** from 334.2 to 279.0 nm, the transitions between terms were calculated to result from splitting in D_{4h} ligand field palladium 4d orbitals. The highest energy range of the spectrum has LMCT character connected with $\pi_{\text{ImCH}} \rightarrow d_{x^2-y^2}/\pi^*_{\text{ImCH}}$ transitions. The difference in the character of the spectra refers to the luminescence of the complexes. Emission properties of the complexes were examined in acetonitrile solutions (with concentration of 1×10^{-3} M dm^{-3}) at room temperature. The solutions of the complexes were excited from 250 to 500 nm, and fluorescence with maximum at 410 nm by excitation at 296 nm was observed only for **2**. Figure 6 presents the fluorescence spectrum. The inset on figure 6 presents a 2D map; in the excitation range 250–450 nm, emission is observed at excitation wavelengths of 296 and 377 nm. The red shift of the emission maximum is typical for 4d metal(II) complexes and emission originating from the charge transfer state is derived from the excitation involving a $d_\pi \rightarrow \pi^*_{\text{ligand}}$ transition. In the calculated electronic spectrum, energy of the $a_{1g}/\pi_{\text{ImCH}} \rightarrow d_{x^2-y^2}/\pi^*_{\text{ImCH}}$ (b_{1g}) transition is close to the energy of the excitation, and it has metal to ligand charge transfer (MLCT) character. The lack of fluorescence in the case of **1** is connected with the absence of MLCT transitions in the range of excitations.

Summarizing, two new cationic palladium(II) complexes with imidazo[1,2-α]pyridine and 1-methylimidazole have been synthesized. The molecular structures of the complexes were determined by X-ray analysis, and infrared, ^{1}H NMR, UV-vis spectra were studied. In both complexes, the ligands coordinate by imidazole nitrogen and the average Pd-N bond distances of 2.008 Å are similar to those reported in the literature for cationic palladium complexes with azole ligands [29–31]. In the crystal structure of **1**, π-stacking interactions are visible as distinct from the crystal structure of **2** in which some interactions

involve the imidazole ring and methyl substituent. In the structure of **2**, water and chloride form chair-like substructures.

Based on the crystal structures, computational studies were carried out to determine the electronic structure. The bond lengths and angles predicted by DFT calculations are different for the two complexes; for **1** the calculated bond lengths are elongated while in **2** shortened, which indicate some differences in electronic structures of the complexes connected with the ligand structures. Electronic spectra of Pd(II) complexes are dominated by charge transfer and intraligand bands, and DFT calculations showed that the HOMO is ligand-dominated.

Electronic spectra were calculated using the TD-DFT method, and the character of the transitions was related to the structure of the molecular orbitals. Emission properties of the complexes have been examined and fluorescence was observed only for **2**. The electronic structures of the complexes showed that contributions of ligands resulted from splitting of the palladium d orbitals in the complexes, the emission originating from the lowest energy MLCT state, derived from the excitation involving a $d_\pi \rightarrow \pi^*_{\text{ligand}}$ transition. In the UV-vis spectrum of **1,** these transitions play a role in the high energy where they are covered by LLCT transitions $(\pi_{\text{impy}} \rightarrow \pi_{\text{impy}^*})$.

Supplementary data

CCDC 782989 and CCDC 820957 contain the supplementary crystallographic data for [Pd(Impy)$_4$]Cl$_2$·2CHCl$_3$ (**1**) and [Pd(ImCH$_3$)$_4$]Cl$_2$·2H$_2$O (**2**), respectively. These data can be obtained free of charge from http://www.ccdc.cam.ac.uk/conts/retrieving.html, or from the Cambridge Crystallographic Data Center, 12 Union Road, Cambridge CB2 1EZ, UK; Fax: (+44) 1223–336-033; or E-mail: deposit@ccdc.cam.ac.uk.

Acknowledgments

The GAUSSIAN09 calculations were carried out in the Wrocław Centre for Networking and Supercomputing, WCSS, Wrocław, Poland (http://www.wcss.wroc.pl).

References

[1] D. Kovala-Demertzi, M.A. Demertzis, E. Filiou, A.A. Pantazaki, P.N. Yadav, J.R. Miller, Y. Zheng, D.A. Kyriakidis. *Biometals*, **16**, 411 (2003).
[2] E. Budizisz, U. Krajewska, M. Rozalski, A. Szulawska, M. Czyż, B. Nawrot. *Eur. J. Pharmacol.*, **502**, 59 (2004).
[3] J. Kuduk-Jaworska, A. Puszko, M. Kibiak, M. Pelczynska. *J. Inorg. Biochem.*, **98**, 1447 (2004).
[4] E. Budzisz, M. Miernicka, I.-P. Lorenz, P. Mayer, U. Krajewska, M. Rozalki. *Polyhedron*, **28**, 637 (2009).
[5] Y. Najajreh, J.M. Perez, C. Navarro-Ranninger, D. Gibson. *J. Med. Chem.*, **45**, 5189 (2002).
[6] E. Khazanov, Y. Barenholtz, D. Gibson, Y. Najajreh. *J. Med. Chem.*, **45**, 5196 (2002).
[7] N. Andrade-Lopez, J.G. Alvarado-Rodrıguez, S. Gonzalez-Montiel, M.G. Rodrıguez-Mendez, M.E. Paez-Hernandez, C.A. Galan-Vidal. *Polyhedron*, **26**, 4825 (2007).
[8] S.O. Ojwach, I.A. Guzei, J. Darkwa, S.F. Mapolie. *Polyhedron*, **26**, 851 (2007).
[9] H. Liang, J. Liu, X. Li, Y. Li. *Polyhedron*, **23**, 1619 (2004).
[10] N.A. Piro, J.S. Owen, J.E. Bercaw. *Polyhedron*, **23**, 2797 (2004).
[11] R. Chen, J. Bacsa, S.F. Mapolie. *Polyhedron*, **22**, 2855 (2003).
[12] L. Ma, R.C. Smith, J.D. Protasiewicz. *Inorg. Chim. Acta*, **358**, 3478 (2005).

[13] E. Guney, V.T. Yilmaz, C. Kazak. *Polyhedron*, **29**, 1285 (2010).
[14] V. Anbalagan, T.S. Srivastava. *Polyhedron*, **23**, 3173 (2004).
[15] M.J. Frisch, G.W. Trucks, H.B. Schlegel, G.E. Scuseria, M.A. Robb, J.R. Cheeseman, G. Scalmani, V. Barone, B. Mennucci, G.A. Petersson, H. Nakatsuji, M. Caricato, X. Li, H.P. Hratchian, A.F. Izmaylov, J. Bloino, G. Zheng, J.L. Sonnenberg, M. Hada, M. Ehara, K. Toyota, R. Fukuda, J. Hasegawa, M. Ishida, T. Nakajima, Y. Honda, O. Kitao, H. Nakai, T. Vreven, J.A. Montgomery, Jr., J.E. Peralta, F. Ogliaro, M. Bearpark, J.J. Heyd, E. Brothers, K.N. Kudin, V.N. Staroverov, R. Kobayashi, J. Normand, K. Raghavachari, A. Rendell, J.C. Burant, S.S. Iyengar, J. Tomasi, M. Cossi, N. Rega, J.M. Millam, M. Klene, J.E. Knox, J.B. Cross, V. Bakken, C. Adamo, J. Jaramillo, R. Gomperts, R.E. Stratmann, O. Yazyev, A.J. Austin, R. Cammi, C. Pomelli, J.W. Ochterski, R.L. Martin, K. Morokuma, V.G. Zakrzewski, G.A. Voth, P. Salvador, J.J. Dannenberg, S. Dapprich, A.D. Daniels, O. Farkas, J.B. Foresman, J.V. Ortiz, J. Cioslowski, D.J. Fox. *Gaussian 09, Revision A.1*, Gaussian, Inc., Wallingford, CT (2009).
[16] A.D. Becke. *J. Chem. Phys.*, **98**, 5648 (1993).
[17] C. Lee, W. Yang, R.G. Parr. *Phys. Rev. B*, **37**, 785 (1988).
[18] M.E. Casida. In *Recent Developments and Applications of Modern Density Functional Theory, Theoretical and Computational Chemistry*, J.M. Seminario (Ed.), Vol. 4, p. 391, Elsevier, Amsterdam (1996).
[19] K. Eichkorn, F. Weigend, O. Treutler, R. Ahlrichs. *Theor. Chem. Acc.*, **97**, 119 (1997).
[20] E.D. Glendening, A.E. Reed, J.E. Carpenter, F. Weinhold. *NBO* (*Version 3.1*) (2001).
[21] N.M. O'Boyle, A.L. Tenderholt, K.M. Langner. *J. Comput. Chem.*, **29**, 839 (2008).
[22] CrysAlis RED, Oxford Diffraction Ltd. (*Version 1.171.29.2*) (2011).
[23] O.V. Dolomanov, L.J. Bourhis, R.J. Gildea, J.A.K. Howard, H. Puschmann. *J. Appl. Crystallogr.*, **42**, 339 (2009).
[24] G.M. Sheldrick. *Acta Crystallogr.*, **A46**, 467 (1990).
[25] K. Wolinski, J.F. Hilton, P. Pulay. *J. Am. Chem. Soc.*, **112**, 8251 (1990).
[26] X.X. Zhang, N. Kobayashi, J.Z. Jiang. *Spectrochim. Acta, Part A*, **64**, 526 (2006).
[27] M.C. Etter, J.C. MacDonald, J. Bersnstein. *Acta Crystallogr.*, **B46**, 256 (1990).
[28] C.F. Macrae, I.J. Bruno, J.A. Chisholm, P.R. Edgington, P. McCabe, E. Pidcock, L. Rodriguez-Monge, R. Taylor, J. van de Streek, P.A. Wood. *J. Appl. Crystallogr.*, **41**, 466 (2008).
[29] Z. Qin, M.C. Jennings, R.J. Puddephatt. *Inorg. Chem.*, **40**, 6220 (2001).
[30] D.J. Hoffart, N.C. Habermehl, S.J. Loeb. *Dalton Trans.*, 2870 (2007).
[31] I. Ara, L.R. Falvello, J. Fornies, R. Lasheras, A. Martin, O. Oliva, V. Sicilia. *Inorg. Chim. Acta*, **359**, 4574 (2006).